J. Fluid Mech. (1998), *vol.* 354, *pp.* 277–299. Printed in the United Kingdom

Compositional convection in the presence of rotation

By I. A. ELTAYEB AND E. A. HAMZA

Department of Mathematics and Statistics, College of Science, PO Box 36, Al-Khodh, Muscat 123, Sultanate of Oman

(Received 21 January 1997 and in revised form 22 May 1997)

The stability of a compositionally buoyant plume, of circular cross-section, rising in a rotating infinite fluid is investigated. Both plume and fluid have the same non-zero kinematic viscosity, ν, and thermal diffusivity, κ. The growth rate of the instability depends on the Taylor number, Ta (which is a dimensionless number measuring the effect of the Coriolis force relative to the viscous force) and on the thickness, s_0, of the plume in addition to the Prandtl number, $\sigma(=\nu/\kappa)$ and the Reynolds number, R (which measures the strength of the forcing). The analysis is restricted to the case of small R. It is found that the presence of rotation enhances instability. A simple model of a single interface separating the two parts of an infinite fluid is investigated first in order to isolate the mechanism responsible for the increase in the growth rate with rotation. It is shown that the Coriolis force interacts with the zonal velocity component to produce a velocity component normal to the interface. For the right choice of wave vector components, this normal velocity component is in phase with the displacement of the interface and this leads to instability. The maximum growth rate is identified in the whole space of the parameters σ, Ta, s_0 when $R \ll 1$. While the maximum growth rate is of order R^2 in the absence of rotation, it is increased to order R in the presence of rotation. It is also found that the Prandtl number, σ, which has a strong influence on the growth rate in the absence of rotation, plays a subservient role when rotation is present.

1. Introduction

The study of convective motions driven by the energy released by the solidification of a component of a fluid alloy has received considerable attention recently because of its relevance to many industrial and geophysical applications (see e.g. Copley *et al.* 1970; Loper 1978, 1983, 1987; Loper & Roberts 1981, 1983; Roberts & Loper 1983; Davis 1990; Huppert 1990; Tait & Jaupart 1992; Worster 1992). When a two-component fluid melt, with the heavier component having the higher melting point, is chilled from below the heavy component solidifies first and settles at the bottom of the container (see, e.g. Hills, Loper & Roberts 1983). The solidification front, however, can suffer morphological instability (Kurz & Fisher 1989) and consequently a thin region develops between the underlying solid and the overlying fluid alloy. This thin region, known as a mush, contains both fluid depleted of the heavy component and solid crystals. As the solidification front advances, the mushy layer thickens and the presence of the buoyant fluid in it makes it unstable. The linear instability of the mushy layer can be of two types. One type occurs in a thin layer on top of the mushy layer and this is associated with very little interaction between the mushy layer and

the overlying fluid. The other type of instability has a larger wavelength and leads to strong interaction between the mushy layer and the overlying fluid (Worster 1992). This latter instability leads to the formation of chimneys in the mushy layer where the buoyant fluid escapes upwards in the form of plumes (see e.g. figure 1 in Eltayeb & Loper 1991) or in the form of blobs (Moffatt & Loper 1994)

Motivated by the geophysical applications, Eltayeb & Loper (1991, 1994, 1997) studied simple models of compositional convection and isolated a mode of instability whose (dimensionless) growth rate is proportional to the square of the Reynolds number, R, when R is small (see (1.2) below). This mode of instability is present for all values of the Prandtl number. The present work extends the study by Eltayeb & Loper (1997) to include the influence of rotation. The motivation for the inclusion of rotation is a geophysical one. Convective motions caused by the solidification of the Earth's inner core are believed to contribute to core motions which interact with the geomagnetic field and help to maintain it. Recent work on the geodynamo suggests that the generation of magnetic fields depends on the small-amplitude asymmetric parts of the field and flow (Lister & Buffett 1995). Although we will not include a magnetic field in the analysis below, rotation plays a crucial role in the dynamics of the Earth's core. Previous studies on double-diffusive fluids (see e.g. Eltayeb 1972) showed that rotation normally plays a stabilizing role. Since the instability identified in the absence of rotation (Eltayeb & Loper 1991) is basically a shear flow instability, the effect of rotation on this mode of instability may not be the same. One of the purposes of this analysis it to investigate the interaction of rotation and shear flow.

A compositionally buoyant column of fluid of radius s_0 is rising in an infinite less-buoyant fluid and both fluids are rotating about the vertical with a uniform angular speed ω. A temperature profile with a vertically constant (and positive) temperature gradient, γ, also varies with the horizontal coordinate. The two fluids possess the same uniform kinematic viscosity, ν,and thermal diffusivity, κ. The stability is then governed by the Taylor number

$$Ta = \left(\frac{2\omega L^2}{\nu}\right)^2 \tag{1.1}$$

in addition to the Reynolds and Prandtl numbers R and σ, respectively, defined by

$$R = \beta\tilde{C}\left(\frac{g\kappa^3}{\alpha^3\gamma^3\nu^5}\right)^{1/4} = \frac{UL}{\nu}, \quad \sigma = \frac{\nu}{\kappa} \tag{1.2}$$

in which $\tilde{C}$ is the amplitude of the basic-state concentration of the light component and α, β, L, U and g are defined in §2 below. Since the Reynolds number is directly proportional to the amplitude of the concentration of light material, the instability is entirely due to the presence of the light material, i.e. the instability is driven by compositional buoyancy.

In §2, we formulate the problem. The study presented below showed that rotation enhances instability. Previous studies have shown that the growth rate of the instability depends on the thickness of the plume as well as on the curvature of the plume surface (Eltayeb & Loper 1994, 1997). In order to clarify this unexpected result we investigate the simple model of a single interface rotating in an infinite fluid in §3. This model rules out the effects of thickness and curvature and allows us to isolate the influence of rotation on the basic physical mechanism driving the instability. For the oblique disturbances, the transverse pressure gradient does not vanish. It is found that this pressure gradient produces a transverse component of velocity which

interacts with the vertical rotation to produce a Coriolis force in the direction normal to the interface. This force produces a component of velocity normal to the interface. Since the interface is a material one, the velocity at the interface is directly related to the displacement. When the wavefront is inclined away from the rotation axis the displacement of the interface is enhanced by the presence of rotation and this promotes instability. As a result, the maximum growth rate is dramatically increased from order R^2 in the absence of rotation to order R when $Ta = O(1)$ and R is small. The instability belongs to oblique modes. For vertical modes the growth rate has the same order of magnitude as in the absence of rotation. In §4, we examine the stability of a cylindrical plume rising in a rotating infinite fluid and clarify the roles played by the thickness of the plume and the curvature of the cylindrical surface. Some concluding remarks are made in §5.

2. Formulation

Consider a fluid of infinite extent rotating uniformly, with angular speed ω, about the vertical. The fluid has density, ρ, which depends on both temperature, T, and concentration, C, of the light component through the relation

$$\rho/\rho_0 = 1 - \alpha(T - T_0) - \beta(C - C_0). \tag{2.1}$$

Here α is the coefficient of thermal expansion and β is a parameter measuring the variations of density with concentration, while T_0, C_0, ρ_0 are reference values. The fluid possesses non-zero kinematic viscosity, ν, and thermal diffusivity κ. The basic equations governing the flow are

$$\rho\left[\frac{\partial \boldsymbol{u}}{\partial t} + (\boldsymbol{u}\cdot\nabla)\boldsymbol{u} + 2\omega\hat{\boldsymbol{z}}\times\boldsymbol{u}\right] = -\nabla p + \rho\nu\nabla^2\boldsymbol{u} - \rho g\hat{\boldsymbol{z}}, \tag{2.2}$$

$$\nabla\cdot\boldsymbol{u} = 0, \tag{2.3}$$

$$\left(\frac{\partial}{\partial t} + \boldsymbol{u}\cdot\nabla\right)T = \kappa\nabla^2 T, \tag{2.4}$$

$$\left(\frac{\partial}{\partial t} + \boldsymbol{u}\cdot\nabla\right)C = 0. \tag{2.5}$$

Here $\boldsymbol{u}$ is the velocity, p the pressure, g the constant gravitational acceleration and $\hat{\boldsymbol{z}}$ is a unit vector directed vertically upwards. In equation (2.5) we have neglected material diffusion.

Define a Cartesian coordinate system $O(x, y, z)$ in which Oz is vertically upwards and Ox, Oy are mutually orthogonal horizontal directions (see figure 1). Equations (2.2)–(2.5) are satisfied by a static solution in which the temperature has a uniform vertical gradient γ:

$$\boldsymbol{u} = 0, \quad C = C_0, \quad \mathrm{d}T/\mathrm{d}z = \gamma. \tag{2.6}$$

We now assume that the light component has a concentration of amplitude $\tilde{C}$. This will induce fluid motions in the fluid. Before we determine these motions, we cast (2.2)–(2.5) in dimensionless form. This is achieved by taking $(\nu\kappa/\alpha\gamma g)^{1/4}$ $(= L)$, $(\kappa/\alpha\gamma\nu g)^{1/2}$ $(= \tau_v)$, $\tilde{C}$, $\beta\tilde{C}(g\kappa/\alpha\gamma\nu)^{1/2}$ $(= U)$, $\beta\tilde{C}/\alpha$, $\rho_0\beta\tilde{C}(g^3\nu\kappa/\alpha\gamma)^{1/4}$ as measures of length, time, compositional difference, velocity, temperature difference and pressure difference, respectively. The length scale defined here is the salt-finger length scale (see e.g. Eltayeb & Loper 1991, hereinafter referred to as EL1) and the time scale

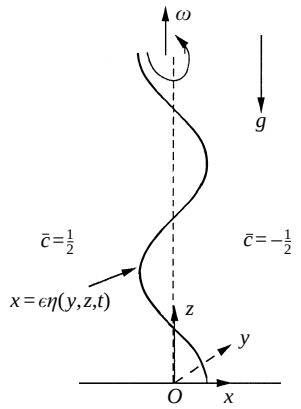

FIGURE 1. The geometry of the single rotating interface model.

corresponds to the viscous time scale

$$\tau_v = L^2/v. \tag{2.7}$$

The dimensionless equations are

$$\frac{\partial \boldsymbol{u}}{\partial t} + R\boldsymbol{u}\cdot\nabla\boldsymbol{u} + Ta^{1/2}\hat{\boldsymbol{z}}\times\boldsymbol{u} = -\nabla(p + z/\beta\tilde{C}) + \nabla^2\boldsymbol{u} + (C - C_0 + T - T_0)\hat{\boldsymbol{z}}, \tag{2.8}$$

$$\nabla\cdot\boldsymbol{u} = 0, \tag{2.9}$$

$$\sigma\left(\frac{\partial}{\partial t} + R\boldsymbol{u}\cdot\nabla\right)T = \nabla^2 T, \tag{2.10}$$

$$\left(\frac{\partial}{\partial t} + R\boldsymbol{u}\cdot\nabla\right)C = 0. \tag{2.11}$$

The three dimensionless parameters σ, R, Ta are known as the Prandtl, Reynolds and Taylor numbers, respectively, and have been defined in §1 above.

We assume that the solutions of (2.8)–(2.11) have the form

$$\boldsymbol{u} = \bar{w}\hat{\boldsymbol{z}} + \epsilon\boldsymbol{u}^\dagger, \quad T = T_b + \bar{T} + \epsilon T^\dagger, \quad p = p_b + \bar{p} + \epsilon p^\dagger, \quad C = C_0 + \bar{C} + \epsilon C^\dagger, \tag{2.12}$$

in which

$$T_b = T_0 + (z - z_0)/\sigma R, \quad p_b = p_0 - (z - z_0)/\beta\tilde{C} + (z - z_0)^2/2\sigma R. \tag{2.13}$$

In (2.12) the variables with an overbar depend on the coordinate, x, normal to the interface only and the † denotes variables depending on space and time, which have a small amplitude ϵ. The remaining terms refer to the static solution. Expressions (2.12) are substituted into (2.8)–(2.11). The terms of order ϵ^0 give

$$0 = -\nabla\bar{p} + (\bar{w}'' + \bar{C} + \bar{T})\hat{\boldsymbol{z}}, \quad \bar{w} = \bar{T}'', \tag{2.14}$$

where the prime denotes differentiation of a basic-state variable with respect to the argument, and the order-ϵ^1 terms yield the linearized perturbation equations:

$$\partial\boldsymbol{u}^\dagger/\partial t + R(\bar{w}\partial\boldsymbol{u}^\dagger/\partial z + \boldsymbol{u}^\dagger\cdot\nabla\bar{w}\hat{\boldsymbol{z}}) + Ta^{1/2}\hat{\boldsymbol{z}}\times\boldsymbol{u}^\dagger = -\nabla p^\dagger + \nabla^2\boldsymbol{u}^\dagger + (C^\dagger + T^\dagger)\hat{\boldsymbol{z}}, \tag{2.15}$$

$$\nabla\cdot\boldsymbol{u}^\dagger = 0, \tag{2.16}$$

$$\sigma\partial T^{\dagger}/\partial t + \sigma R(\bar{w}\partial T^{\dagger}/\partial z + (\boldsymbol{u}^{\dagger}\cdot\hat{\boldsymbol{x}})\bar{T}') + \boldsymbol{u}^{\dagger}\cdot\hat{\boldsymbol{z}} = \nabla^2 T^{\dagger}, \tag{2.17}$$

$$(\partial/\partial t + R\bar{\omega}\partial/\partial z)C^{\dagger} = 0. \tag{2.18}$$

3. Stability of the rotating single interface

In this section we utilize the perturbation equations (2.15)–(2.18) to study the linear stability of the solutions (3.3) below in the presence of rotation. Our interest here concerns the instabilities driven by the difference in composition of the fluid on either side of the interface at $x = 0$. It turns out that instabilities occur for small values of the Reynolds number R. We shall then assume that

$$R \ll 1. \tag{3.1}$$

We prescribe the concentration profile

$$\bar{C} = -\tfrac{1}{2}\mathrm{sgn}(x) \tag{3.2}$$

so that a sudden jump in concentration occurs at $x = 0$.

The basic-state equations (2.14) are independent of rotation, because the basic flow is parallel to the angular velocity, and the solution is the same as that obtained for the non-rotating case (EL1, §3). We include it here for the benefit of the reader:

$$\left.\begin{aligned} \bar{\omega}^{\pm} &= -\tfrac{1}{2}\exp(\mp x/\sqrt{2})\sin(x/\sqrt{2}), \\ \bar{T}^{\pm} &= \pm\tfrac{1}{2}\{1 - \exp(\mp x/\sqrt{2})\cos(x/\sqrt{2})\}. \end{aligned}\right\} \tag{3.3}$$

The upper (lower) superscript is used to identify the solution in the interval $x > 0 (x < 0)$, respectively. A full discussion of this solution is given in EL1.

The interface is disturbed so that it has the profile

$$x = \epsilon\eta(y, z, t) = \epsilon\eta_0 \exp(\mathrm{i}(my + nz) + \Omega t) + \text{c.c.} \tag{3.4}$$

See figure 1. The perturbations (2.12) are strongly coupled to the interface. In general, it is possible to consider disturbances which are not coupled to the interface, as can be inferred from studies of the similar problem of a heated vertical wall (see e.g. Holyer 1983) in the absence of rotation. However, instabilities associated with such disturbances occur for order-1 values of the Reynolds number R and hence are less unstable than the coupled disturbances studied here which suffer instability for small values of R. We then assume that

$$\{\boldsymbol{u}^{\dagger}, p^{\dagger}, T^{\dagger}, C^{\dagger}\} = \{\mathrm{i}nu(x), nv(x), w(x), \mathrm{i}np(x), T(x), C(x)\}\exp(\mathrm{i}(my+nz)+\Omega t)+\text{c.c.} \tag{3.5}$$

The perturbation equations (2.15)–(2.18) can then be written in component form

$$(\mathrm{L} - \Omega_*)u - \mathrm{i}Ta^{1/2}v - \mathrm{D}p = 0, \tag{3.6}$$

$$(\mathrm{L} - \Omega_*)v - \mathrm{i}Ta^{1/2}u + mp = 0, \tag{3.7}$$

$$(\mathrm{L} - \Omega_*)w - \mathrm{i}R\bar{w}'u + C + T + n^2 p = 0, \tag{3.8}$$

$$(\mathrm{L} - \sigma\Omega_*)T - \mathrm{i}R\bar{T}'nu - w = 0, \tag{3.9}$$

$$\mathrm{D}u + mv + w = 0, \tag{3.10}$$

$$\Omega_* C = 0, \tag{3.11}$$

where

$$\mathrm{D} \equiv \mathrm{d}/\mathrm{d}x, \quad \mathrm{L} \equiv \mathrm{D}^2 - a^2, \quad a^2 = m^2 + n^2, \tag{3.12}$$

and the Doppler-shifted 'frequency' is defined by

$$\Omega_* = \Omega + \mathrm{i}nR\bar{w}(x). \tag{3.13}$$

Since Ω_* depends on x, (3.11) demands that

$$C = 0. \tag{3.14}$$

The perturbation variables are excited by the disturbance of the interface and must all decay to zero away from the interface. The variables must also satisfy certain conditions at the interface. The interface must be a material surface. The full variables (basic + perturbation) and their derivatives must be continuous and the fluxes of momentum and heat must also be continuous at the interface. The boundary conditions on the perturbation variables can then be summarized as

$$u, v, w, T, p \to 0 \quad \text{as} \quad x \to \pm\infty, \tag{3.15a}$$

$$u, v, w, T, p, \mathrm{D}T, \mathrm{D}v \quad \text{are continuous at} \quad x = 0, \tag{3.15b}$$

$$\mathrm{D}w(0_-) - \mathrm{D}w(0_+) = 1, \tag{3.15c}$$

$$\mathrm{i}Rnu(0) = \Omega, \tag{3.15d}$$

where in (3.15*d*) we have used the fact that $\bar{w}(0) = 0$ so that (3.13) gives $\Omega_* = \Omega$ on the interface.

The method of solution, as described in EL1, is by expansion in the small parameter R:

$$\Omega = \sum_{r=1}^{\infty} \Omega_r R^r, \quad f = \sum_{r=0}^{\infty} f_r R^r, \tag{3.16}$$

where f stands for any of the perturbation variables u, v, w, T, p. The expansion (3.16) is substituted into (3.6)–(3.10) and the boundary conditions (3.15) and the different powers of R are equated to zero to obtain a hierarchy of systems of equations which can be solved successively.

The presence of rotation is represented by the terms proportional to $Ta^{1/2}$ in (3.6) and (3.7). It will be shown below that the presence of the Coriolis force leads to a dramatic change in the stability properties of the interface. To proceed gradually towards identifying the stability of the rotating single interface, let us examine the case of small rotation rate first.

3.1. *The effect of small rotation on the stability of the interface*

The study of the stability of the interface in the absence of rotation carried out in EL1 showed that the stability is determined, to leading order, by considering the systems of equations corresponding to R^0 and R^1. It follows then from (3.6), (3.7), (3.15) and (3.16), that rotation will contribute to the stability problem provided that $Ta^{1/2} \geqslant O(R)$. We then assume that

$$Ta^{1/2} = \Gamma R \tag{3.17}$$

with $\Gamma = O(1)$ in order to examine the influence of small rotation on the stability of the interface. The analysis is carried out in the same way as in EL1.† For the benefit of the reader we mention the main points here. When the expansions (3.16) are substituted into (3.6)–(3.10) and the boundary conditions (3.15) and the coefficients of $R^r (r = 0, 1, 2, \ldots)$ are equated to zero, the first two systems of equations and the

† This derivation is not published in EL1 but derived at a later stage. The full details of the derivations can be obtained from either of the authors of EL1.

associated boundary conditions are sufficient to determine the stability to leading order.

When $r = 0$, we obtain the set of equations

$$\mathrm{L}p_0 - T_0 = 0, \quad \mathrm{L}w_0 + T_0 + n^2 p_0 = 0, \quad \mathrm{L}T_0 - w_0 = 0, \tag{3.18a–c}$$

$$\mathrm{L}u_0 - \mathrm{D}p_0 = 0, \quad \mathrm{L}v_0 - mp_0 = 0. \tag{3.18d,e}$$

The associated boundary conditions are obtained from (3.15) by attaching a subscript 0 to all the variables and replacing Ω by Ω_1. The solution of (3.18) can then be written as

$$\{u_0^{\pm}, v_0^{\pm}, w_0^{\pm}, p_0^{\pm}, T_0^{\pm}\} = \sum_{j=1}^{3} \{\mp\lambda, -m, \mu_j^3, \mu_j, \mu_j^2\} A_j \mathrm{e}^{\mp\lambda_j x}, \tag{3.19}$$

where

$$A_j = \frac{\mu_j^2}{2\lambda_j(3n^2 + 2\mu_j)}, \quad \mu_j = \lambda_j^2 - a^2, \tag{3.20}$$

and μ_j are the roots of the cubic equation

$$\mu^3 + \mu + n^2 = 0. \tag{3.21}$$

We also find from (3.15*d*) that

$$\Omega_1 = 0. \tag{3.22}$$

The next system of equations is

$$\mathrm{L}p_1 - T_1 = F_p, \quad \mathrm{L}w_1 + T_1 + n^2 p_1 = F_w, \quad \mathrm{L}T_1 - w_1 = F_T, \tag{3.23a–c}$$

$$\mathrm{L}u_1 - \mathrm{D}p_1 = F_u, \quad \mathrm{L}v_1 - mp_1 = F_v, \tag{3.23d,e}$$

where

$$F_p = -2\mathrm{i}\bar{w}' u_0, \quad F_w = \mathrm{i}\bar{w}' u_0 + \mathrm{i}\bar{w} u_0, \quad F_T = \mathrm{i}\sigma(\bar{T}' u_0 + \bar{w} T_0), \tag{3.24a–c}$$

$$F_u = \mathrm{i}(n\bar{w} u_0 + \Gamma v_0), \quad F_v = \mathrm{i}(n\bar{w} v_0 + \Gamma u_0). \tag{3.24d,e}$$

The associated boundary conditions are obtained from (3.15) by attaching a subscript 1 to all the variables in (3.15*a–c*), by replacing the right-hand side of (3.15*c*) by 0 and by writing (3.15*d*) as

$$\mathrm{i}nu_2 = \Omega_2. \tag{3.25}$$

Since the homogeneous part of (3.23) is identical to (3.18), we will not proceed to solve (3.23). We derive the solvability condition which will provide an expression for the growth rate Ω_2. This can be done as follows. Multiply (3.23*d*) by $\exp(-ax)$, integrate from $x = 0$ to $x = \infty$ and use the boundary conditions to get

$$\Omega_2 = \frac{n}{a}\int_0^\infty \bar{w}(x) u_0(x) \mathrm{e}^{-ax} \mathrm{d}x + \frac{\Gamma}{a}\int_0^\infty v_0(x)\mathrm{e}^{-ax}\mathrm{d}x - \mathrm{i}n\int_0^\infty p_1 \mathrm{e}^{-ax}\mathrm{d}x. \tag{3.26}$$

Next we use (3.23*a–c*) to find that

$$\mathrm{L}^3 p_1 + \mathrm{L}p_1 + n^2 p_1 = \mathrm{L}^2 F_p + \mathrm{L}F_T + F_p + F_w. \tag{3.27}$$

Multiply both sides of (3.27) by

$$\exp(-ax) - \sum_{j=1}^{3} \frac{n^2 \exp(-ax)}{3n^2 + 2\mu_j} \tag{3.28}$$

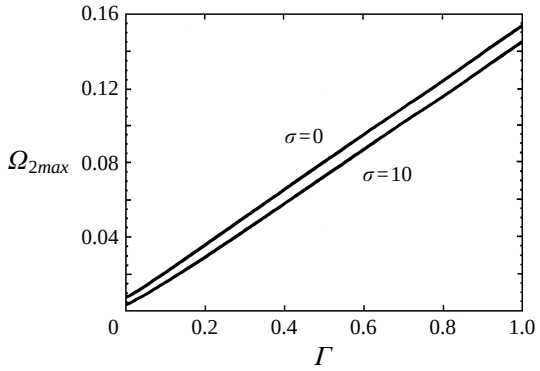

FIGURE 2. The dependence of the maximum growth rate on Γ for small rotation rates. Note that the curve is almost linear and the variations with Prandtl number σ are very small.

and integrate from $x = 0$ to $x = \infty$ and use the boundary conditions to get

$$n^2 \int_0^\infty p_1 \mathrm{e}^{-ax}\mathrm{d}x = \int_0^\infty (F_p + F_w)\mathrm{e}^{-ax}\mathrm{d}x - \sum_{j=1}^{3} \frac{n^2}{3n^2 + 2\mu_j} \int_0^\infty (\mu_j^2 F_p + \mu_j F_T + F_p + F_w)\mathrm{e}^{-\lambda_j x}\mathrm{d}x. \quad (3.29)$$

We now use (3.29) to eliminate the last integral from (3.26) to obtain an expression for the growth rate Ω_2, which can be written in the form

$$\Omega_2 = \Omega_{20} + \Gamma\,\Omega_{2T} \quad (3.30)$$

in which Ω_{20} is the expression obtained in the absence of rotation (see (4.30) in EL1), and

$$\Omega_{2T} = \frac{n}{a}\int_0^\infty v_0 \mathrm{e}^{-ax}\mathrm{d}x = -\frac{mn}{a}\sum_{j=1}^{3}\frac{A_j}{\lambda_j + a}. \quad (3.31)$$

The growth rate Ω_2, as given in (3.30), was maximized over m and n for different values of σ and Γ. When $\Gamma = 0, m$ and n occur in the forms m^2 and n^2, and the maximum growth rate, as calculated in EL1, is independent of the signs of m and n. For non-zero rotation rates, the combination mn appears as a multiplicative factor in the expression for Ω_{2T}, which is the contribution due to the presence of rotation. We must therefore consider both the cases (i) $mn > 0$ and (ii) $mn < 0$. The results show that when $mn < 0$, the growth rate increases with the increase of Γ. The increase is linear as suggested by (3.30) which means that the contribution of the factor corresponding to Γ dominates, even when $\Gamma < 1.0$. This is shown in figure 2, which also illustrates the influence of the Prandtl number on the maximum growth rate, Ω_{2max}. Although the Prandtl number has little influence on the growth rate, it has a marked influence on the wavenumbers m and n, as illustrated in figure 3. When $mn > 0$, on the other hand, the growth rate is damped by the presence of rotation.

The contribution Ω_{2T} to the growth rate is entirely due to the presence of the last term in F_u, as given in (3.23) and (3.24). This term affects the velocity $u^\dagger$ normal to the interface and $u^\dagger$ affects the displacement, η, of the interface according to

$$\frac{\mathrm{d}\eta}{\mathrm{d}t} = Ru^\dagger(0, y, z, t). \quad (3.32)$$

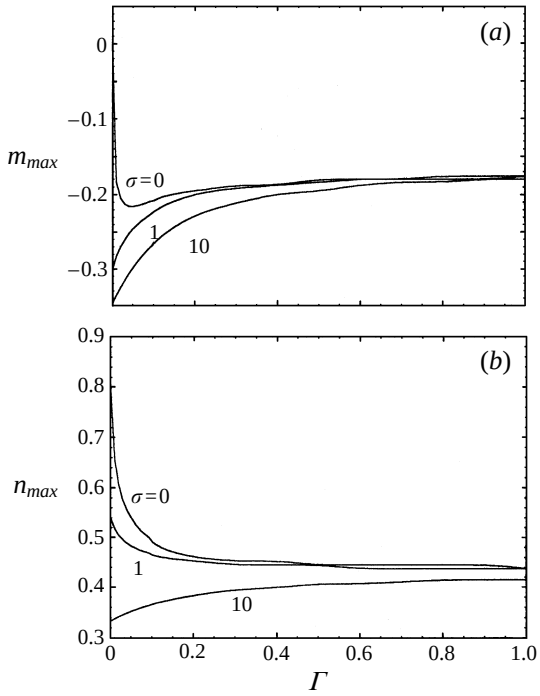

FIGURE 3. The variations of the wavenumbers of the preferred mode with Γ for different values of σ. Note that both wavenumbers vary rapidly with Γ when Γ is small but they soon attain steady values as Γ increases beyond about 0.5.

If the contribution to $u^\dagger$ in the absence of rotation is $u_0^\dagger$ and the contribution due to the presence of rotation is $Ta^{1/2}u_T^\dagger$ then

$$u^\dagger = u_0^\dagger + Ta^{1/2}u_T^\dagger. \tag{3.33}$$

The contribution $u_T^\dagger$ is due to the interaction of vertical rotation with the zonal flow $v^\dagger$, as indicated by (3.23*d*) and (3.24*d*). From (3.19) we see that $v^\dagger$ is proportional to m which measures the inclination of the wavefront to the vertical. In the absence of rotation there is symmetry with respect to the vertical and m occurs in the form m^2 in the expression for the growth rate, and there is no preference for either sign of m. In the presence of rotation a vertical component of vorticity is introduced (see equation (3.39) below) and this has the effect of destroying the symmetry in m. The vertical vorticity due to rotation tilts the wavefront away from the vertical (i.e. away from the axis of rotation) and $u_T^\dagger$ thus produced is in phase with η, resulting in the growth of the displacement of the interface. This situation corresponds to $mn < 0$. If $mn > 0$ then $u_T^\dagger$ is out of phase with η and the disturbance is damped.

The linear increase of Ω_{2max} with Γ suggests that when $Ta = O(1)$, the dependence of the growth rate on R is different from that for $\Gamma = 0$. We will discuss the case $Ta = O(1)$ next.

3.2. *The stability of the rotating interface*

When $Ta = O(1)$, we find it convenient to scale v in the fashion

$$v = Ta^{1/2}\tilde{v}, \tag{3.34}$$

and define the scaled vertical component of vorticity, $\zeta^\dagger$, by

$$\zeta^\dagger = -\mathrm{i}\hat{\boldsymbol{z}} \cdot \mathrm{curl}\boldsymbol{u}^\dagger / nTa^{1/2}, \tag{3.35}$$

so that $\zeta^\dagger$ has the same dependence as the other variables in (3.5). The scaling in (3.34) and (3.35) as well as that used in (3.5) is made to avoid the proliferation of the parameters $i, n, Ta^{1/2}$ in the equations below. We now use (3.6)–(3.8) and (3.10) to find an equation for the pressure. The set of equations (3.6)–(3.10) can conveniently be written in the form

$$\mathrm{L}w + T + n^2 p = RF_w, \tag{3.36}$$

$$\mathrm{L}T - w = RF_T, \tag{3.37}$$

$$\mathrm{L}p - T - Ta\zeta = RF_p, \tag{3.38}$$

$$\mathrm{L}\zeta + w = RF_\zeta, \tag{3.39}$$

$$(\mathrm{D}^2 - m^2)\tilde{v} = \mathrm{i}\mathrm{D}\zeta + mTa^{-1/2}w, \tag{3.40}$$

$$\mathrm{D}u = -mTa^{1/2}\tilde{v} - w, \tag{3.41}$$

where

$$F_w = \mathrm{i}\bar{w}' nu + R^{-1}\Omega_* w, \quad F_T = \mathrm{i}\sigma\bar{T}' nu + \sigma R^{-1}\Omega_* T, \tag{3.42}$$

$$F_p = -2\mathrm{i}\bar{w}' nu, \quad F_\zeta = nTa^{-1/2}\bar{w}'\tilde{v} + \Omega_*\zeta R^{-1}. \tag{3.43}$$

We substitute the expansion (3.16) into (3.36)–(3.41) and equate the coefficients of $R^r (r = 1, 2 \ldots)$ to zero. The leading-order set of equations is obtained by attaching a subscript '0' to all the perturbation variables in (3.36)–(3.41) and the boundary conditions (3.15), and replacing the right-hand sides of (3.36)–(3.39) by zero. The equations resulting from (3.36)–(3.39) give

$$\nabla^6 w_0 + \nabla^2 w_0 + n^2(1 - Ta)w_0 = 0. \tag{3.44}$$

The method of solution is straightforward. Equation (3.44) gives w_0 and T_0, ζ_0, p_0, v_0 and u_o are obtained from (3.37), (3.39), (3.38), (3.40) and (3.41), respectively, provided we set the right-hand sides of (3.37)–(3.39) to zero. We find

$$\{w_0^\pm, T_0^\pm, p_0^\pm\} = \sum_{j=1}^{3} \{\mu_j^3, \mu_j^2, \mu_j(1 - Ta)\} A_j \mathrm{e}^{\mp\lambda} j^x, \tag{3.45}$$

$$\{u_0^\pm, \tilde{v}_0^\pm\} = \sum_{j=1}^{3} \{\pm\mu_j\lambda_j + \mathrm{i}mTa^{1/2}, mTa^{-1/2}\mu_{j^\pm}\mathrm{i}\lambda_j\} \frac{A_j\mu_j^2}{\mu_j + n^2} \mathrm{e}^{\mp\lambda} j^x. \tag{3.46}$$

Here

$$A_j = \frac{\mu_j^3 - n^2 Ta}{2\lambda_j\mu_j[2\mu_j + 3n^2(1 - Ta)]} \tag{3.47}$$

and μ_j, λ_j are given by

$$\mu_j^3 + \mu_j + n^2(1 - Ta) = 0, \quad \lambda_j^2 = \mu_j + a^2 \tag{3.48}$$

such that $\mathrm{Re}(\lambda_j) > 0$. Since the cubic equation (3.48) has real coefficients, it possesses one real root and two complex conjugate roots. It can then be shown that

$$\sum_{j=1}^{3} f(\mu_j, \lambda_j, A_j) \tag{3.49}$$

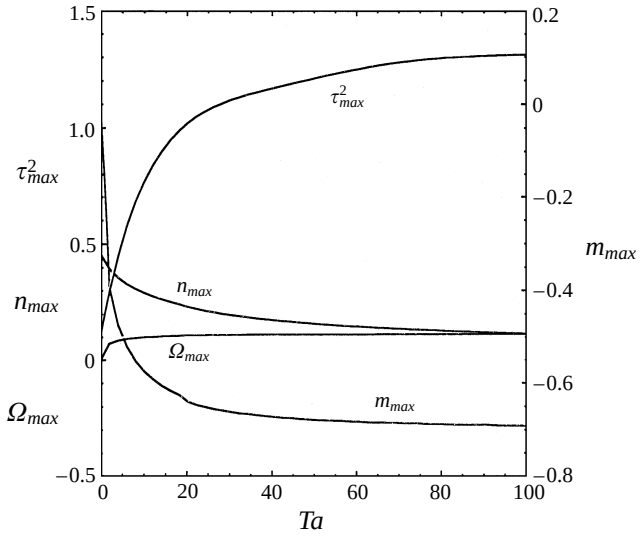

FIGURE 4. The mode of maximum growth rate for the rotating single interface. As Ta increases from zero, the growth rate increases sharply at first and then approaches an asymptote at 0.113; the vertical wavenumber decreases moderately at first and then slowly for large Ta; the zonal wavenumber (negative) increases in magnitude sharply at first and then more slowly. The corresponding value of τ increases sharply at first and then slowly towards an asymptote at 1.22.

is always real for arbitrary function f provided that it does not contain any complex constants. If we further use (3.47) and (3.48), we find

$$\sum_{j=1}^{3} \frac{\mu_j^3 \lambda_j A_j}{\mu_j + n^2} = 0, \tag{3.50}$$

The growth rate Ω_1, according to the boundary condition (3.15d) together with the first of (3.46) and (3.50), is given by

$$\Omega_1 = -mnTa^{1/2} \sum_{j=1}^{3} \frac{A_j \mu_j^2}{\mu_j + n^2}. \tag{3.51}$$

According to (3.49) this expression, whose presence is wholly due to the effect of rotation, is purely real. Consequently, the influence of rotation is to increase the growth rate to order R from order R^2 in the absence of rotation. Computations of (3.51) showed that the growth rate has a positive maximum which is associated with $mn < 0$, confirming the predictions of the small-Ta results obtained above. In fact (3.51) arises from the second term in the expression for $u_0^{\pm}$ given by (3.46) which is due to the second term in the expression for $v_0^{\pm}$ in (3.46) which is brought about by the presence of the vertical vorticity $\zeta_0^{\pm}$ in (3.40).

A sample of the results for the maximum growth rate, Ω_{max}, and the associated vertical and transverse wavenumbers, n_{max} and m_{max}, respectively, is given in figure 4. As Ta increases from zero, the maximum growth rate increases linearly and sharply at first but when Ta reaches order 10 values it increases more slowly and approaches an asymptote as Ta tends to infinity. This is confirmed by noting that the magnitude

of n_{max} decreases steadily with Ta. An asymptotic analysis for $Ta \to \infty$ gives

$$\Omega_1 = m\tau \sum_{j=1}^{3} \mu_j / \{2(2\mu_j - 3\tau^2)(\mu_j + m^2)^{1/2}\}; \quad \tau = nTa^{1/2}. \tag{3.52}$$

This expression was maximized over τ and m to find that the maximum, Ω_{max}, of Ω_1 and the associated values, τ_{max} and m_{max}, of τ and m are

$$\Omega_{max} = 0.113295, \quad \tau_{max} = 1.22344, \quad m_{max} = -0.70781. \tag{3.53}$$

It then follows that the zonal wavenumber m_{max} remains of order 1 while

$$n_{max} \simeq 1.22344 Ta^{-1/2}; \quad Ta \to \infty. \tag{3.54}$$

It should be noted here that we have assumed $n > 0$ and $m < 0$. The reverse will give the same growth rate.

Figure 4 also shows the dependence of n_{max}, m_{max} and τ_{max} on Ta. The 'zonal' wavenumber m_{max} of the maximum growth rate increases in magnitude but remains negative and greater than -0.8. The vertical wavenumber n_{max} on the other hand decreases steadily with Ta and takes the asymptotic form (3.54) as Ta increases indefinitely, so that the wavelength parallel to rotation increases as $Ta^{1/2}$. Also τ_{max} increases sharply at first but approaches a constant value, as in (3.53), when $Ta \to \infty$. Of course τ_{max} is not relevant to the maximum growth rate when $Ta = O(1)$ but the whole range of Ta is included in order to illustrate how the limit in (3.53) is reached.

The results of this section show that rotation has a destabilizing effect on the vertical interface, and the maximum growth rate, Ω_{max}, is order R in the presence of rotation as compared to the order of magnitude R^2 in the absence of rotation. This applies only for oblique disturbances. When the disturbance propagates vertically (i.e. when $m = 0$) then it can be shown that $\Omega_{max} = O(R^2)$, and rotation does not change the asymptotic dependence of the growth rate on R, although it can increase the numerical value of Ω/R^2 for certain values of the Prandtl number σ.

3.3. *Energy considerations*

The role played by the new term in u can also be clarified by appealing to energy considerations. Multiply equations (3.6), (3.7) and (3.8) by u^*, v^* and w^* (where a superstar here refers to the complex conjugate), respectively , integrate and use (3.15) to get

$$\Omega E_M = -D_M + B + J + nR(M - \mathrm{i}E_{WU}) - \mathrm{i}n^2 Ta E_\omega. \tag{3.55}$$

Here the term on the left-hand side represents the rate of change of wave kinetic energy, D_M defines the rate of viscous dissipation, M the rate of transfer of kinetic energy from the mean flow to the wave through the velocity shear, B and J represent the rates of gain of wave energy by the actions of thermal and compositional buoyancy, respectively, and E_ω is the wave energy due to the Coriolis force. These are defined by

$$E_M = \int_{-\infty}^{\infty} |\boldsymbol{u}|^2 \mathrm{d}x, \quad D_M = \int_{-\infty}^{\infty} \left\{ \left| \frac{\mathrm{d}\boldsymbol{u}}{\mathrm{d}t} \right|^2 + a^2 |\boldsymbol{u}|^2 \right\} \mathrm{d}x, \tag{3.56a,b}$$

$$M = -\mathrm{i} \int_{-\infty}^{\infty} \bar{w}' w^* u \mathrm{d}x, \quad E_{WU} = \int_{-\infty}^{\infty} \bar{w} |\boldsymbol{u}|^2 \mathrm{d}x, \tag{3.56c,d}$$

$$B = \int_{-\infty}^{\infty} w^* T \mathrm{d}x, \quad E_\omega = \int_{-\infty}^{\infty} (u\bar{v}^* + u^* \bar{v}) \mathrm{d}x, \tag{3.56e,f}$$

$$J = w^*(0)\left(\frac{\mathrm{d}w(0_-)}{\mathrm{d}x} - \frac{\mathrm{d}w(0_+)}{\mathrm{d}x}\right). \tag{3.56g}$$

If we multiply the complex conjugate of (3.9) by T and integrate, we find

$$\sigma\Omega^* E_T = -D_T - B + \sigma Rn(H + \mathrm{i}E_{WT}) \tag{3.57}$$

where

$$E_T = \int_{-\infty}^{\infty} |T|^2 \mathrm{d}x, \quad D_T = \int_{-\infty}^{\infty} \left\{ \left| \frac{\mathrm{d}T}{\mathrm{d}x} \right|^2 + a^2 |T|^2 \right\} \mathrm{d}x \tag{3.58a,b}$$

$$H = \mathrm{i} \int_{-\infty}^{\infty} \bar{T}' u^* T \mathrm{d}x, \quad E_{WT} = \int_{-\infty}^{\infty} \bar{w} |T|^2 \mathrm{d}x. \tag{3.58c,d}$$

Here E_T is the gain in wave potential energy, D_T the rate of thermal dissipation of energy and H is the rate of transfer of energy to the wave by the temperature gradient .

Adding (3.55) to (3.57) and taking the real and imaginary parts, we obtain

$$\mathrm{Re}(\Omega)[E_M + \sigma E_T] = -(D_T + D_M) + \mathrm{Re}(J) + nR\mathrm{Re}(M + \sigma H), \tag{3.59}$$

$$\mathrm{Im}(\Omega)[E_M - \sigma E_T] = \mathrm{Im}(J) + nR\mathrm{Im}(M + \sigma H) + nR(\sigma E_{WT} - E_{WU}) - n^2 Ta E_\omega. \tag{3.60}$$

We can now use the expansion (3.16) in (3.59) and (3.60), noting that in view of (3.15*c*) the expression for J takes the form $J = w^*(0)$, to obtain for the first two terms in the expansion

$$-(D_M^{(0)} + D_T^{(0)}) + \mathrm{Re}(w_0^*(0)) = 0, \quad \mathrm{Im}(w_0^*(0)) = n^2 Ta E_\omega^{(0)}, \tag{3.61a,b}$$

$$\mathrm{Re}(\Omega_1)[E_M^{(0)} + \sigma E_T^{(0)}] = -(D_M^{(1)} + D_T^{(1)}) + n\mathrm{Re}(M^{(0)} + \sigma H^{(0)}) + \mathrm{Re}(w_1^*(0)), \tag{3.62a}$$

$$\mathrm{Im}(\Omega_1)[E_M^{(0)} - \sigma E_T^{(0)}] = n(\sigma E_{WT}^{(0)} - E_{WU}^{(0)}) + n\mathrm{Im}(M^{(0)} + \sigma H^{(0)}) + \mathrm{Im}(w_1^*(0)) - n^2 Ta E_\omega^{(1)}. \tag{3.62b}$$

Equation (3.61*b*) is automatically satisfied by the expressions (3.45) and (3.46) for w_0, u_0 and v_0 while (3.61*a*) represents a balance between compositional buoyancy on the one hand and both thermal and viscous diffusions on the other. Equation (3.62*a*) shows that the growth rate $\mathrm{Re}(\Omega_1)$ is a result of the excess energy from compositional buoyancy, as represented by w_1^*, and from the release of energy by the basic flow, as represented by M, and temperature gradient, through the presence of H, over the dissipation of energy by thermal and viscous diffusions. In the absence of rotation, the right-hand side of (3.62*a*) vanishes and the growth rate is zero to this order of approximation. However, when rotation is present, the even part of the leading-order flow normal to the interface which is introduced by the presence of rotation, contributes to $M^{(0)}$ and $H^{(0)}$ as well as to $w_1(0)$, and leads to a non-zero right-hand side which is positive when $mn < 0$.

The single interface has provided a simple example to illustrate the destabilizing influence of rotation. In the next section we study the more realistic model of a cylindrical plume in order to examine the role played by the thickness of the plume and the curvature of the plume surface.

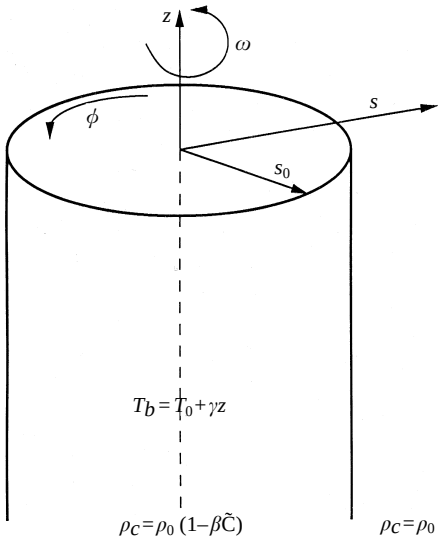

FIGURE 5. The geometry of the cylindrical plume.

4. The cylindrical plume

Consider a compositional plume in the form of a right circular cylinder of radius s_0. We consider a cylindrical system of coordinates (s, ϕ, z) with the z-axis pointing vertically upwards along the axis of the plume, s is radially outwards and ϕ is the zonal angle (see figure 5).

The basic-state concentration is taken as the top-hat profile

$$\bar{C} = \begin{cases} 1 & \text{for} \quad s < s_0 \\ 0 & \text{for} \quad s > s_0. \end{cases} \tag{4.1}$$

The plume is rotating uniformly about the vertical with uniform angular velocity ω. The basic state which was given and discussed in EL1 (see also (4.25) below), is associated with both the vertical flow, $\bar{w}(s)$, and temperature, $\bar{T}(s)$, being even in s. The temperature is negative on the axis $s = 0$ and increases monotonically with s to 0 as $s \to \infty$. $\bar{T}(0)$ decreases with the increase of s_0 and approaches -1.2 as s_0 increases indefinitely. The vertical flow, $\bar{w}(s)$, is oscillatory in s, takes positive values on the axis and decays to zero for large s. $\bar{w}(0)$ oscillates with the radius of the plume and attains an overall maximum when s_0 is near 2.0. The buoyancy flux of the basic state also attains a maximum value when s_0 is near 2.0.

The perturbation equations are given in (2.15)–(2.18). For the purpose of the analysis in this section, we find it convenient to write them in the form

$$\nabla p^\dagger + \mathrm{curl}^2 \boldsymbol{u}^\dagger - T^\dagger \hat{\boldsymbol{z}} + Ta^{1/2} \hat{\boldsymbol{z}} \times \boldsymbol{u}^\dagger = -R\boldsymbol{F}^\dagger, \tag{4.2}$$

$$\nabla^2 T^\dagger - \boldsymbol{u}^\dagger \cdot \hat{\boldsymbol{z}} = RG^\dagger, \tag{4.3}$$

$$\nabla \cdot \boldsymbol{u}^\dagger = 0, \tag{4.4}$$

where

$$\boldsymbol{F}^\dagger = \frac{1}{R}\frac{\partial \boldsymbol{u}^\dagger}{\partial t} + \bar{w}\frac{\partial \boldsymbol{u}^\dagger}{\partial z} + \boldsymbol{u}^\dagger \cdot \nabla \bar{w} \hat{\boldsymbol{z}}, \quad G^\dagger = \frac{\sigma}{R}\frac{\partial T^\dagger}{\partial t} + \sigma\left(\bar{w}\frac{\partial T^\dagger}{\partial z} + \boldsymbol{u}^\dagger \cdot \nabla \bar{T}\right). \tag{4.5}$$

The perturbation in concentration, $C^\dagger$, also vanishes here.

The disturbed profile of the interface at $s = s_0$ takes the form

$$s = s_0 + \epsilon\eta(\varphi, z, t), \quad \eta(\varphi, z, t) = \eta_0 \exp(\Omega t + \mathrm{i}nz + \mathrm{i}q\varphi) + \text{c.c.} \tag{4.6}$$

See figure 5. The fact that the instability is entirely due to the disturbance of the interface allows us to write

$$\{\boldsymbol{u}^\dagger, p^\dagger, T^\dagger\} = \{\boldsymbol{u}(s), p(s), T(s)\} \exp(\Omega t + \mathrm{i}nz + \mathrm{i}q\varphi) + \text{c.c.} \tag{4.7}$$

We shall always use the superscript † to refer to variables containing the exponential, while variables without this superscript will be considered to be functions of s only.

We now introduce the toroidal and poloidal parts of the velocity by

$$\boldsymbol{u}^\dagger = \mathrm{curl}(U^\dagger \hat{\boldsymbol{z}}) + \mathrm{curl}^2(V^\dagger \hat{\boldsymbol{z}}) \tag{4.8}$$

so that (4.4) is automatically satisfied. We next apply the operators $\hat{\boldsymbol{z}} \cdot \mathrm{curl}$, $\hat{\boldsymbol{z}} \cdot \mathrm{curl}^2$ and $\nabla\cdot$ to (4.2) and use (4.8) in (4.3) to find that the perturbation equations take the form

$$\Delta(\nabla^2 U^\dagger + \mathrm{i}nTa^{1/2} V^\dagger) = -R\hat{\boldsymbol{z}} \cdot \mathrm{curl}\, \boldsymbol{F}^\dagger, \tag{4.9}$$

$$\Delta(\nabla^4 V^\dagger - \mathrm{i}nTa^{1/2} U^\dagger - T^\dagger) = R\hat{\boldsymbol{z}} \cdot \mathrm{curl}^2 \boldsymbol{F}^\dagger, \tag{4.10}$$

$$\nabla^2 p^\dagger - \mathrm{i}nT^\dagger + Ta^{1/2}\Delta U^\dagger = -R\nabla \cdot F^\dagger, \tag{4.11}$$

$$\nabla^2 T^\dagger + \Delta^\dagger V^\dagger = RG^\dagger, \tag{4.12}$$

in which

$$\Delta = \nabla^2 - \partial^2/\partial z^2 \tag{4.13}$$

and ∇^2 is the usual Laplacian in cylindrical coordinates. According to (4.8), the vertical velocity $w^\dagger$, the radial component of velocity $u^\dagger$ and the zonal component $v^\dagger$ are given by

$$w^\dagger = -\Delta V^\dagger, \quad u^\dagger = \mathrm{i}qs^{-1} U^\dagger + \mathrm{i}n\partial V^\dagger/\partial s, \quad v^\dagger = -\partial U^\dagger/\partial s - nqV^\dagger/s. \tag{4.14}$$

The boundary conditions appropriate to the cylindrical geometry are:

$$\boldsymbol{u}, T, p \text{ are analytic}, \tag{4.15a}$$

$$u, T, p, \mathrm{d}v/\mathrm{d}s, \mathrm{d}T/\mathrm{d}s \text{ are continuous across } s = s_0, \tag{4.15b}$$

$$\mathrm{d}w(s_{0-})/\mathrm{d}s - \mathrm{d}w(s_{0+})/\mathrm{d}s = 1, \tag{4.15c}$$

$$Ru = \Omega + \mathrm{i}nR\bar{w}(s_0). \tag{4.15d}$$

As we have already shown in the case of the single interface, the stability problem is determined, to leading order, by the zero-order terms in the perturbation equations (4.9)–(4.12). Neglecting the right-hand sides, the equations give (suppressing the exponential part)

$$\mathrm{M}^3 V_0 + \mathrm{M}V_0 + n^2(1 - Ta)V_0 = 0, \tag{4.16}$$

in which

$$\mathrm{M} \equiv \frac{\mathrm{d}^2}{\mathrm{d}s^2} + \frac{1}{s}\frac{\mathrm{d}}{\mathrm{d}s} - n^2 - \frac{q^2}{s^2}. \tag{4.17}$$

This equation has constant coefficients and its solution can be written in terms of modified Bessel functions. The application of the boundary conditions (4.15*a–c*) leads

to the solution

$$[V_0, U_0, T_0, p_0] = s_0 \sum_{j=1}^{3} B_j[\mu_j^2, -\mathrm{i}nTa^{1/2}\mu_j, -\xi_j^2\mu_j, -\mathrm{i}n(1-Ta)\xi_j^2]K_q(\xi_j s_0)I_q(\xi_j s) \quad (4.18)$$

for $s < s_0$; and

$$[V_0, U_0, T_0, p_0] = s_0 \sum_{j=1}^{3} B_j[\mu_j^2, -\mathrm{i}nTa^{1/2}\mu_j, -\xi_j^2\mu_j, -\mathrm{i}n(1-Ta)\xi_j^2]I_q(\xi_j s_0)K_q(\xi_j s) \quad (4.19)$$

for $s > s_0$. Here μ_j ($j = 1,2,3$) is given by

$$\mu_j^3 + \mu_j + n^2(1-Ta) = 0, \quad (4.20)$$

and

$$\xi_j^2 = \mu_j + n^2, \quad B_j = \frac{1}{2\mu_j + 3n^2(1-Ta)}. \quad (4.21)$$

In (4.21), ξ_j must be chosen such that $\mathrm{Re}(\xi_j) > 0$. The remaining boundary condition, (4.15*d*), gives an expression for Ω_1. If we note that replacing A_j by B_j in (3.49) leads to a real expression also, we have

$$\Omega_1 = -\mathrm{i}n\Omega_i + nqTa^{1/2}\Omega_g, \quad (4.22)$$

in which Ω_i and Ω_g are real and given by

$$\Omega_i = \bar{w}(s_0) - s_0 \sum_{j=1}^{3} B_j\xi_j\mu_j^2 I_q'(\xi_j s_0)K_q(\xi_j s_0), \quad (4.23)$$

$$\Omega_g = \sum_{j=1}^{3} B_j\mu_j I_q(\xi_j s_0)K_q(\xi_j s_0). \quad (4.24)$$

In (4.23), $\bar{w}(s)$ is the basic upward plume flow given by (see EL1, §3)

$$\bar{w} = \mathrm{Im}(\tilde{w}), \quad \tilde{w} = \begin{cases} -ks_0K_1(ks_0)I_0(ks) & \text{for} \quad s < s_0, \\ ks_0I_1(ks_0)K_0(ks) & \text{for} \quad s_0 < s, \end{cases} \quad (4.25)$$

where

$$k = (1+\mathrm{i})/\sqrt{2} \quad (4.26)$$

Expression (4.22) reduces to that obtained for the non-rotating plume by Eltayeb & Loper (1997) when $Ta = 0$. The presence of rotation introduces the extra term Ω_g which is real and it imparts a growth rate of order R to the disturbance. If Ω_g is positive then the plume is unstable while negative values of Ω_g give stability. The preferred mode of instability is the maximum possible positive value of Ω_g taken over all possible values of the wavenumbers n and q, for any fixed s_0 and Ta. It is to be noted that the Prandtl number does not appear in the expression for the growth rate and therefore the stability is independent of the Prandtl number, to leading order.

Expression (4.22) was evaluated numerically. The computations showed that Ω_g is positive for a whole range of values of n, q, s_0 and Ta. The maximum growth rate, Ω_{max}, of Ω_g and the associated values, n_{max} and q_{max}, of n and q were identified in the (s_0, Ta)-plane. Again it was found that the preferred mode is associated with $nq < 0$. The computations were carried out for $n < 0$ and $q > 0$. Reversing the signs of n and q will yield the same growth rate. The main features of the stability

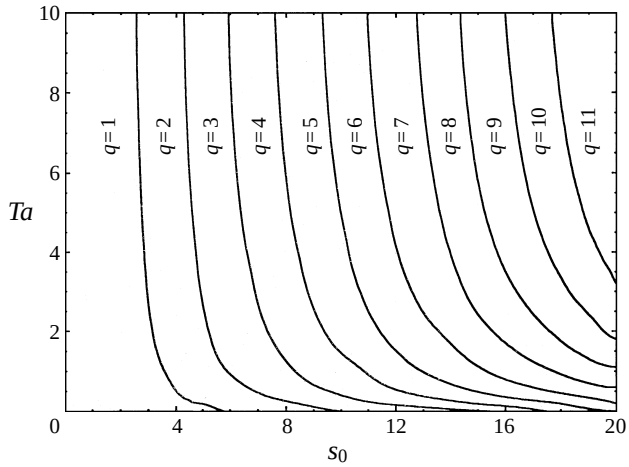

FIGURE 6. The regions of the (Ta, s_0)-plane where the discrete zonal wavenumbers are preferred. The region labelled $q = N$ represents the domain in which the maximum growth rate is associated with a zonal wavenumber $q_{max} = N$. The maximum vertical wavenumber in the various region is illustrated in figures 7–9.

are illustrated in figures 6–9. Figure 6 summarizes the dependence of the stability on the zonal wavenumber q_{max}. The asymmetry of the preferred mode, as measured by q_{max}, increases with the radius of the plume, s_0. As s_0 increases to infinity, q_{max} increases proportionately so that q/s_0 remains of order unity and the plume matches with the single interface. The dependence of the maximum growth rate, Ω_{max}, and the associated vertical wavenumber, n_{max}, on Ta in the various regions defined by q_{max} on Ta and s_0 are quite similar. Some samples of the results are presented in figures 7–9. In figure 7, we see that Ω_{max} increases sharply with Ta when Ta is small and more slowly for values of Ta in excess of about 5. The growth rate is almost the same for values of s_0 more than about 5, although the values of q_{max} change with the increase of s_0. The wavenumber n_{max} decreases with Ta, whatever the value of q_{max}. The dependence of Ω_{max} and n_{max} on s_0 is illustrated in figures 8 and 9. For moderate values of Ta, Ω_{max} increases sharply from 0 at $s_0 = 0$ with $q_{max} = 1$ until s_0 is about 2.5 and thereafter Ω_{max} increases slowly with q_{max} jumping to the next higher integer after an interval of about 2 (see figure 8*a*). Figure 8(*b*) shows the behaviour of n_{max}. For every value of q_{max}, n_{max} decreases with s_0. However, the decrease is sharper for smaller values of q_{max}. Figure 9 illustrates the dependence of Ω_{max}, q_{max} and τ_{max} on s_0 when $Ta \to \infty$. Here the asymptotic law

$$\tau = nTa^{1/2} = O(1), \quad Ta \to \infty \tag{4.27}$$

applies for n. The maximum growth rate Ω_{max} increases more sharply (than for moderate Ta) with s_0 when s_0 is small and the intervals for which the various values of q_{max} are preferred become shorter. The behaviour of n_{max} with s_0 is similar to that found for moderate values of Ta.

The imaginary part, Ω_i, of Ω_1, as given in (4.22) and (4.23), is non-zero. Unlike the single interface where the basic flow vanishes on the interface, the cylindrical plume has, in general, non-zero basic flow on the interface. The imaginary part of Ω_1 does not vanish so that the perturbations can accommodate the harmonic deflection of the interface. Now Ω_i depends on both n and q and gives rise to the vertical phase speed,

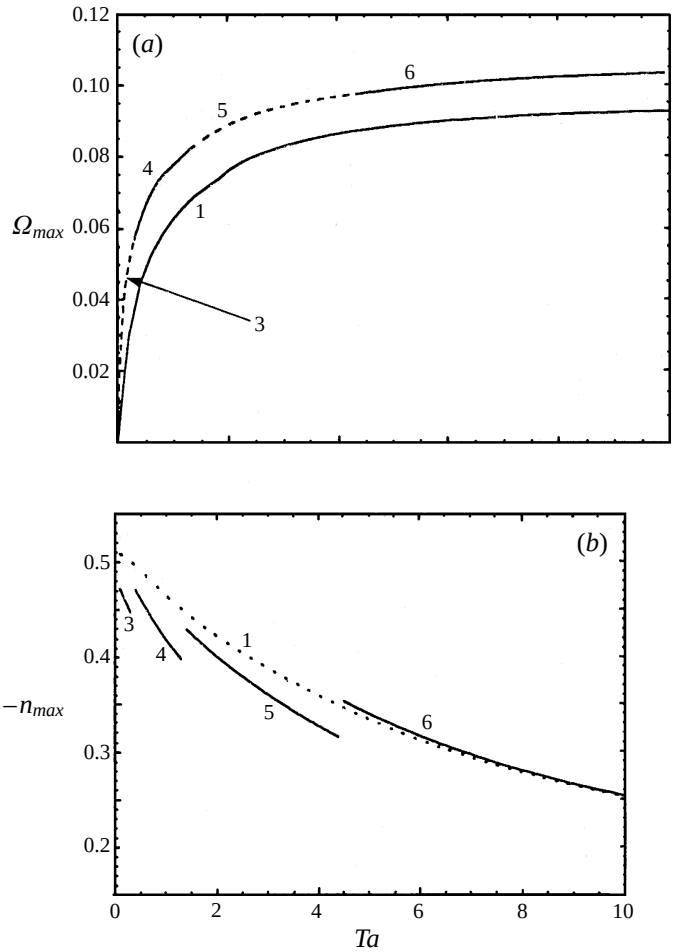

FIGURE 7. The dependence of the maximum growth rate, Ω_{max}, and the associated vertical wavenumber, n_{max}, on the Taylor number. In (a) the upper and lower curves refer to Ω_{max} when $s_0 = 5.0$ and $s_0 = 2.0$, respectively. The arabic numerals refer to the values of q_{max} corresponding to that range of s_0. For all values of s_0 the growth rate increases sharply for small Ta but more slowly for Ta in excess of about 5. The change in q_{max} can also be deduced from figure 6. The continuous and discontinuous parts are used alternately in order to clarify the sections relevant to the different values of q_{max}. In (b) the dotted curve corresponds to $s_0 = 2.0$ and the others to $s_0 = 5.0$.

U_z, and the zonal phase speed, U_φ, defined by

$$U_z = \Omega_i, \quad U_\varphi = (n/q)\Omega_i. \tag{4.28}$$

It follows immediately from (4.28) that U_z and U_ϕ are related by

$$U_z = (q/n)U_\varphi. \tag{4.29}$$

Since $nq < 0$ then U_z and U_ϕ always have different signs. This means that the phase propagation is either clockwise up the plume or anticlockwise down the plume. Figure 10 gives the isolines of the zonal phase speed, U_φ, in the (s_0, n)-plane for $Ta = 20$. It is found that the shapes of the contours do not change very much with q but the numerical values decrease with the increase in q. It is also found that the zonal phase speed is positive for the range of values of n relevant to the maximum

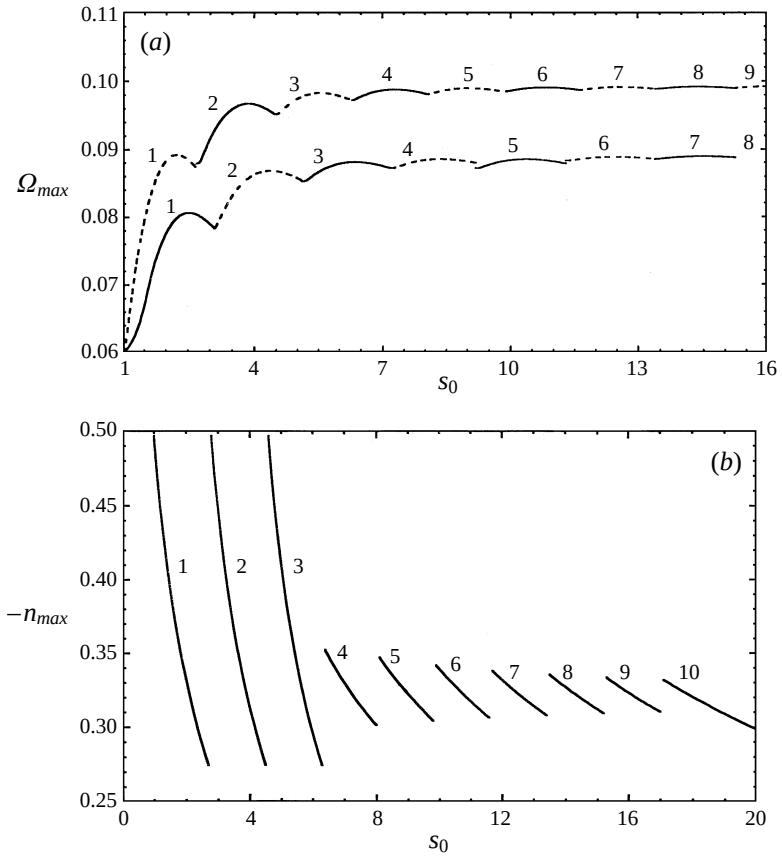

FIGURE 8. The dependence of the growth rate, Ω_{max}, and the vertical wavenumber, n_{max}, on s_0. In both (*a*) and (*b*) the numbers refer to the corresponding values of q_{max}. In (*a*) the upper (lower) curves refer to $Ta = 5.0$ ($Ta = 2.0$). The growth rate increases sharply from zero (when $s_0 = 0$) with s_0 for small s_0 and is almost constant for s_0 greater than about 10. The continuous and discontinuous parts are used alternately in order to clarify the sections relevant to the different values of q_{max}. In (*b*) the curves for $Ta = 5.0$ only are shown. Note that the vertical wavenumber decreases more rapidly when s_0 is small.

growth rate. Consequently the unstable waves propagate in the prograde direction. Since U_z and U_φ have different signs, vertical phase propagation of the unstable waves is downwards. The unstable waves then propagate anticlockwise downwards.

5. Concluding remarks

The stability of a vertical circular cylindrical compositional plume rising in an infinite less-buoyant fluid, with the plume and fluid rotating uniformly about the vertical, has been studied in the case of small Reynolds number. In the absence of rotation Eltayeb & Loper (1997) have shown that the plume is prone to instability for small values of the Reynolds number R, which is directly proportional to the amplitude of the concentration of the light material. They found that the maximum growth rate (providing the preferred mode of instability) is proportional to R^2. It is shown here that the presence of rotation enhances the instability of the plume. The rotation rate is measured by the dimensionless Taylor number Ta. For moderate and

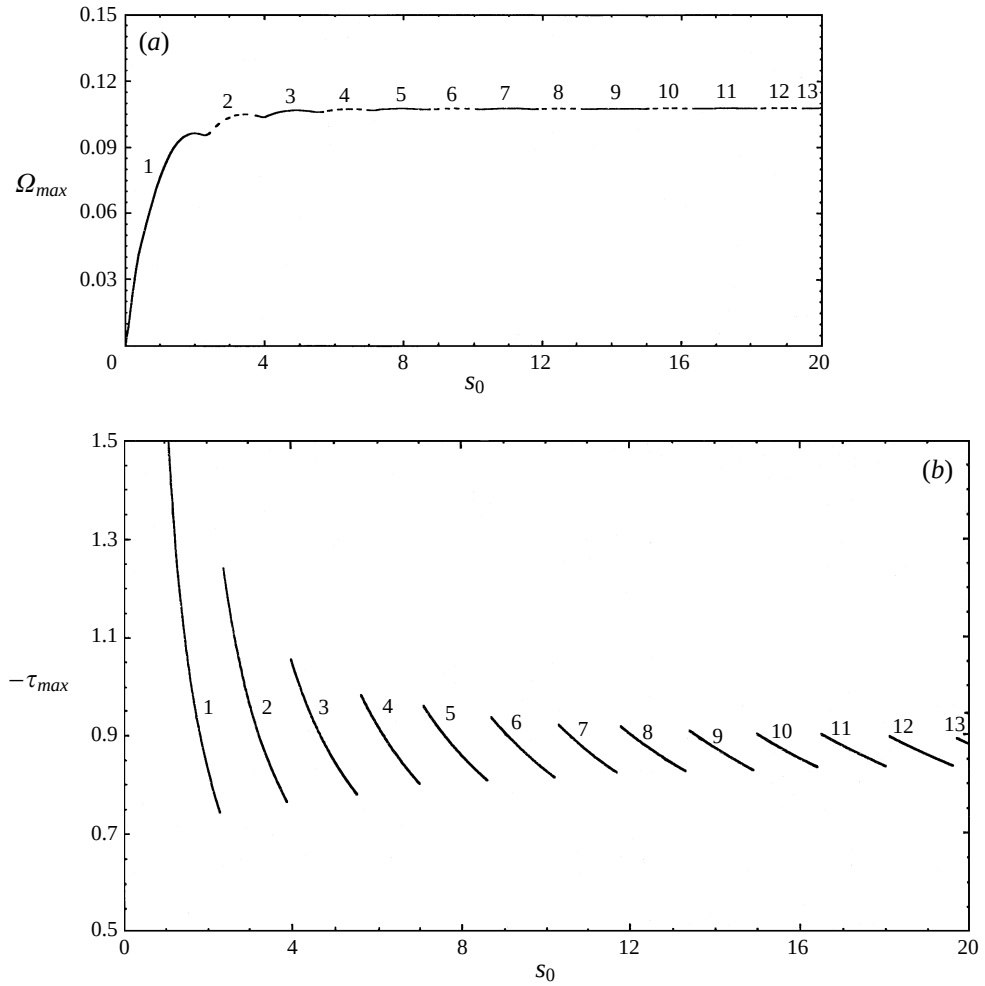

FIGURE 9. The maximum growth rate, Ω_{max}, and the associated scaled vertical wavenumber, τ_{max} as functions of s_0, when Ta is very large. In (a) the continuous and discontinuous parts are used alternately in order to clarify the sections relevant to the different values of q_{max}.

large Ta, the maximum growth rate is proportional to R, so that it is asymptotically larger than in the absence of rotation. The preferred mode is, as in the absence of rotation, oscillatory with a phase speed of the order R so that the period of oscillation is

$$\tau_{osc} = \frac{L}{U} = \frac{\nu}{U^2} = \frac{\nu\rho}{(\Delta\rho)_c g L}, \tag{5.1}$$

where $(\Delta\rho)_c$ is the jump in density associated with the jump in concentration. This order of magnitude is the same as that obtained in the absence of rotation. The time scale of growth, τ_{grow}, of the disturbance here has the same order of magnitude as (5.1) and is very different from that obtained in the absence of rotation.

The instability is necessarily three-dimensional. The product nq of the vertical wavenumber n and the zonal wavenumber q must be strictly negative. The mechanism responsible for the instability can be traced to the interaction between the zonal component of velocity and the vertical rotation. This interaction gives rise to a

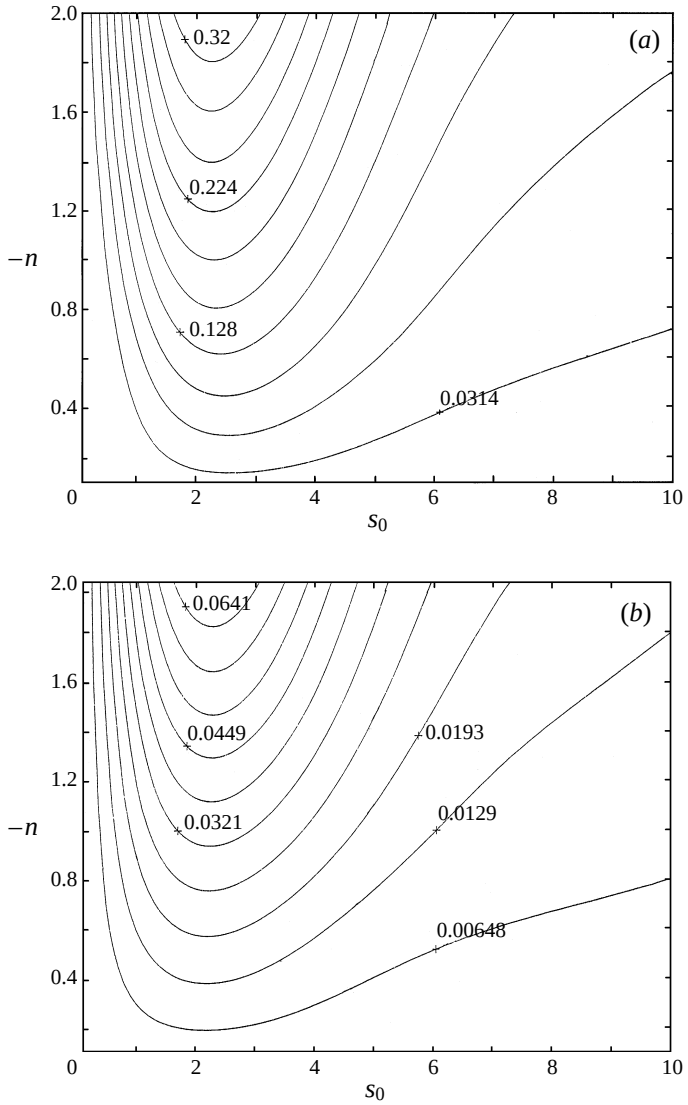

FIGURE 10. The isolines of the zonal phase speed U_φ in the (s_0, n)-plane when $Ta = 2.0$ for (*a*) $q = 1$ and (*b*) $q = 5$. Note that the contours are similar but the numerical values are smaller for larger q.

Coriolis force normal to the interface separating the plume from the surrounding fluid. This force produces a velocity component normal to the interface. Since the interface is a material surface, this normal component is directly related to the displacement of the interface (see (3.32) above). Since the zonal component of the perturbation velocity is proportional to the zonal wavenumber, the Coriolis force is most effective when the disturbance propagates at an angle to the interface. If $nq < 0$, the wave front is inclined away from the interface and the displacement of the interface is enhanced, thus leading to instability.

The analysis presented above may have relevance to conditions at the surface of the inner core of the Earth where small-scale motions may ensue as a result of the settling of the solidified heavy iron component in the iron-rich fluid alloy forming

the outer core of the Earth. Near the inner core boundary, the thermal diffusivity is 4.2×10^{-6} m s^{-2}, the coefficient of thermal expansion is 6.7×10^{-6} s^{-1}, acceleration due to gravity is 4.4 m s^{-2} and the temperature gradient is about 2.3×10^{-4} K m^{-1} (Stacey, 1992, pp. 454, 459). The viscosity of the Earth's outer core is very uncertain and can be assumed to vary between 10^{-7} m^2 s^{-1} and 10^2 m^2 s−1 (Acheson & Hide 1973, p. 202). We then find that L varies between 0.05 m and 50.6 m while Ta varies between 10^{-8} and 10.2. The results obtained above showed that instability occurs for the whole range of values of the parameter Ta and this makes it difficult to rule out the relevance of the plumes to the geodynamo. However, the Reynolds number R may be large in which case the instabilities are likely to be nonlinear. It would then be of interest to investigate the nonlinear development of the plumes. Such a study may clarify the manner in which the unstable waves evolve and whether the unstable waves can break up the plume into blobs which rise to the surface of the outer core. In such a case these motions may contribute to dynamo generation (Moffatt 1992). On the other hand, the presence of a magnetic field may modify the linear stability results obtained here. It may then be more plausible to examine the influence of the magnetic field on the linear stability of the plume before a nonlinear analysis can be attempted. This will be reported in another publication.

I.A.E. wishes to thank Professors A. M. Soward and C. A. Jones (University of Exeter) for some helpful comments during the IAGA Scientific Assembly, Buenos Aires, in August 1993. We also wish to thank the anonymous referees for their constructive comments on an earlier version of the paper.

REFERENCES

Acheson, D. J. & Hide, R. 1973 Hydromagnetics of rotating fluids. *Rep. Prog. Phys.* **36**, 159–221.

Copley, S. M., Giamel, A. F., Johnson, S. M. & Hornbecker, M. F. 1970 The origin of freckles in unidirectionally solidified castings. *Metall. Trans.* **1**, 2193–2204.

Davis, S. H. 1990 Hydrodynamic interactions in directional solidification. *J. Fluid Mech.* **212**, 241–262.

Eltayeb, I. A. 1972 Hydromagnetic convection in a rapidly rotating layer *Proc. R. Soc. Lond.* A **326**, 229–254.

Eltayeb, I. A & Loper, D. E. 1991 On the stability of vertical double-diffusive interfaces. Part 1. A single plane interface. *J. Fluid Mech.* **228**, 149–181 (referred to herein as EL1).

Eltayeb, I.A. & Loper, D. E. 1994 On the stability of vertical double-diffusive interfaces. Part 2. Two parallel interfaces. *J. Fluid Mech.* **267**, 251–273.

Eltayeb, I. A & Loper, D. E. 1997 On the stability of vertical double-diffusive interfaces. Part 3. Cylindrical interface. *J. Fluid Mech.* **353**, 45–66.

Hills, R. N., Loper, D. E. & Roberts, P. H. 1983 A thermodynamically consistent model of a mushy zone. *Q. J. Mech. Appl. Maths* **36**, 505–539.

Holyer, J. Y. 1983 Double diffusive interleaving due to horizontal gradients. *J. Fluid Mech.* **137**, 347–362.

Huppert, H. E. 1990 The fluid mechanics of solidification. *J. Fluid Mech.* **212**, 209–240.

Kurz, W. & Fisher, D. J. 1989 *Fundamentals of Solidification.* Trans. Tech.

Lister, J. R. & Buffett, B. A. 1995 The strength and efficiency of thermal and compositional convection in the geodynamo. *Phys. Earth Planet. Inter.* **91**, 17–30.

Loper, D. E. 1978 The gravitationally powered dynamo. *Geophys. J. R. Astron. Soc.* **54**, 389–404.

Loper, D. E. 1983 Structure of the inner core boundary. *Geophys. Astrophys. Fluid Dyn.* **25**, 139–155.

Loper, D. E. (Ed.) 1987 *Structure and Dynamics of Partially Solidified Systems.* Matinus Nijhoff.

Loper, D. E. & Roberts, P. H. 1981. A study of conditions at the inner-core boundary of the Earth. *Phys. Earth Planet. Inter.* **24**, 302–307.

Loper, D. E. & Roberts, P. H. 1983 Compositional convection and the gravitationally powered dynamo. In *Stellar and Planetary Magnetism* (ed. A. M. Soward), pp. 297–327. Gordon and Breach.

Moffatt, H. K. 1992 The Earth's magnetism: past achievements and future challenges. *IUGG Union Lectures, Vienna 1991*, pp. 1–19, Am. Geophys. Union, Washington, DC.

Moffatt, H. K & Loper, D. E. 1994 The magnetostrophic rise of a buoyant parcel in the Earth's core. *Geophys. J. Intl* **117**, 394–402.

Roberts, P. H. & Loper, D. E. 1983 Towards a theory of the structure and evolution of a dendrite layer. In *Stellar and planetary magnetism* (ed. A. M. Soward), pp. 329–349. Gordon and Breach.

Stacey, F. D. 1992 *Physics of the Earth.* Brookfield Press, Brisbane.

Tait, S. & Jaupart, C. 1992 compositional convection in a reactive crystalline mush and melt differentiation. *J. Geophys. Res.* **97**, 6735–7656.

Worster, M. G. 1992 Instabilities of the liquid and mushy regions during solidification of alloys. *J. Fluid Mech.* **237**, 649–669.